Supplementary Material

Lewis acid activating CO_2 reduction over Ni modified Ni-Ge hydroxide driven by visible-infrared light

Zhenyu Xin,‡[a] Lei Lu,‡[a] Bing Wang,[b] Xiaohui Wang,[a] Kai Zhu,[c] Zhe Xu,[a] Zhentao Yu,[a] Shicheng Yan,*[a] and Zhigang Zou[a,b]

[a.] Eco-materials and Renewable Energy Research Center (ERERC),
National Laboratory of Solid State Microstructures, Collaborative Innovation Center of Advanced Microstructures, College of Engineering and Applied Sciences, Nanjing University, 210093 (P. R. China)
[b.] Jiangsu Province Key Laboratory for Nanotechnology, School of Physics, Nanjing University, Nanjing, Jiangsu 210093 (P. R. China)
[c.] School of Information Science and Engineering, Nanjing University Jinling College, No. 8 Xuefu Road, Nanjing, Jiangsu 210089, P. R. China
*Corresponding author E-mail address: yscfei@nju.edu.cn (Shicheng Yan)
‡These authors contributed equally to this work.

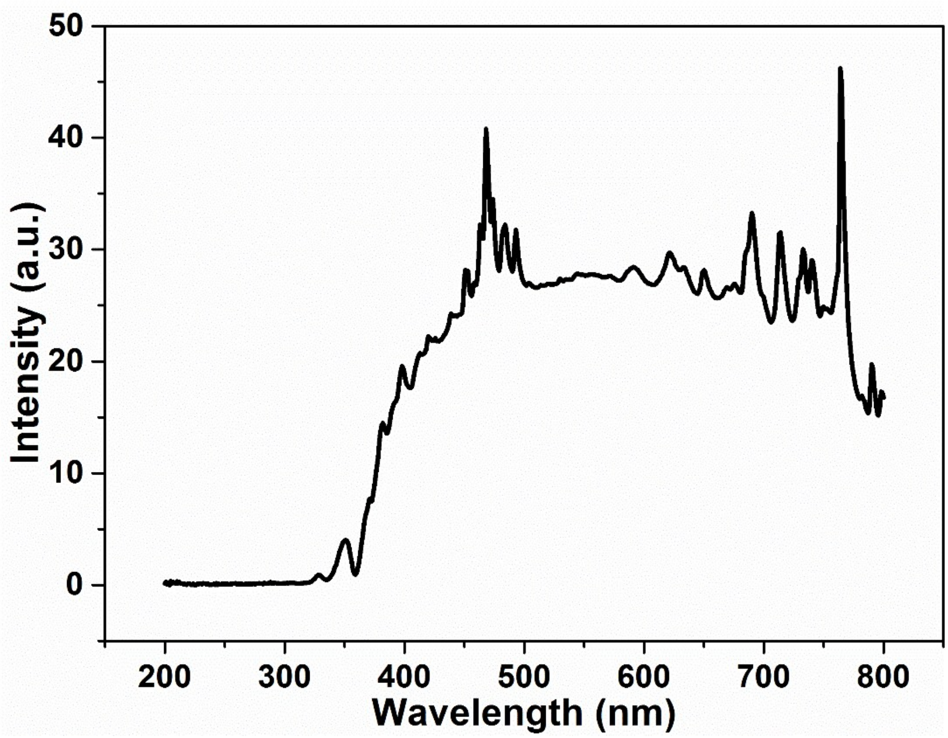

Fig. S1. Radiation spectrum of 300 W Xe lamp used in this study as light source.

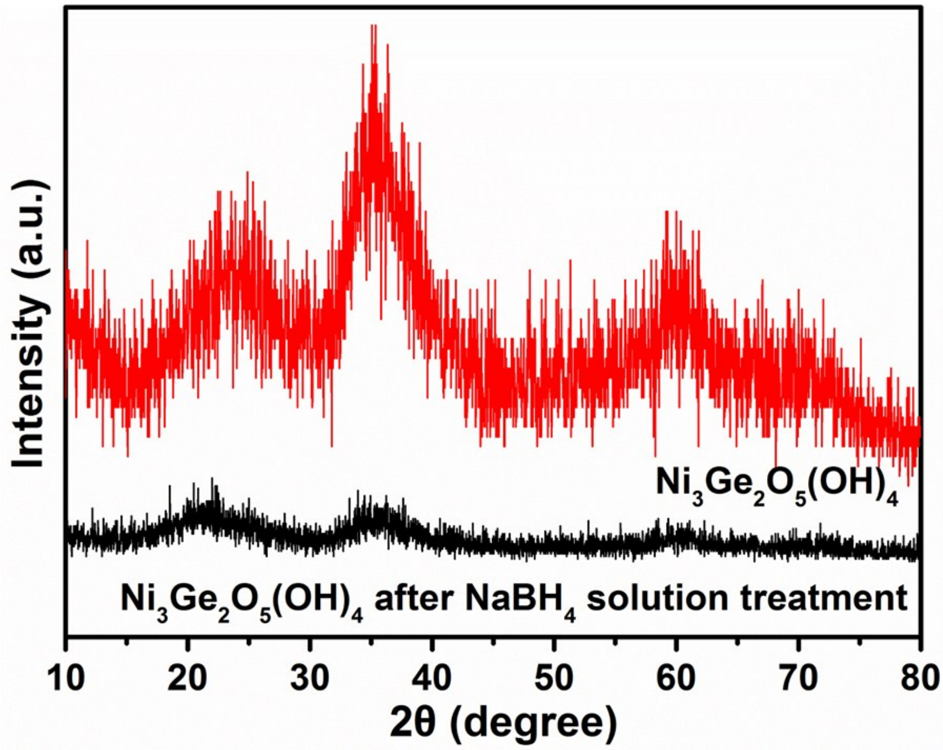

Fig. S2. XRD patterns of $Ni_3Ge_2O_5(OH)_4$ and $Ni_3Ge_2O_5(OH)_4$ after $NaBH_4$ solution treatment.

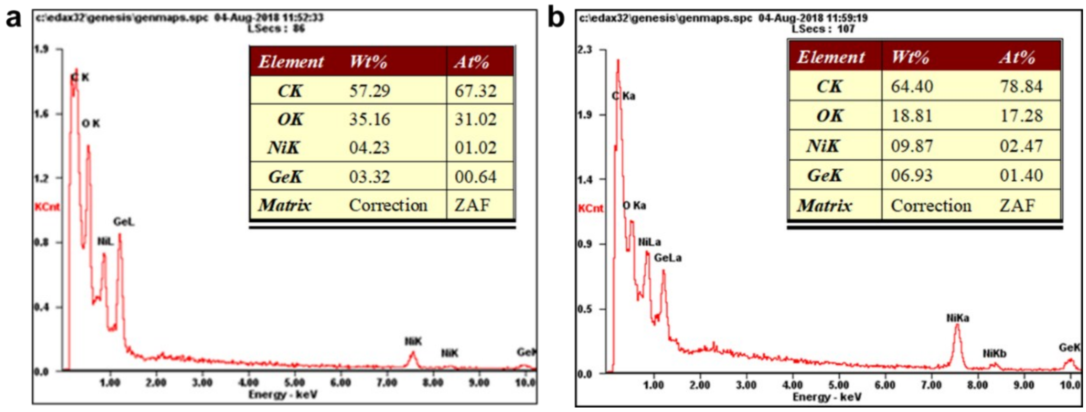

Fig. S3. EDS analysis of the (a) $Ni_3Ge_2O_5(OH)_4$ and (b) $Ni/Ni_3Ge_2O_5(OH)_4$. For $Ni_3Ge_2O_5(OH)_4$, n(Ni) / n(Ge) = 1.02 / 0.64 = 1.59. For $Ni/Ni_3Ge_2O_5(OH)_4$, n(Ni) / n(Ge) = 2.47 / 1.40 = 1.76. The theoretical atom ratio of Ni:Ge in the $Ni_3Ge_2O_5(OH)_4$ and $Ni/Ni_3Ge_2O_5(OH)_4$ are 1.50 and $\frac{n(Ni^{2+}) + n(Ni^0)}{\frac{2}{3}n(Ni^{2+})}$.

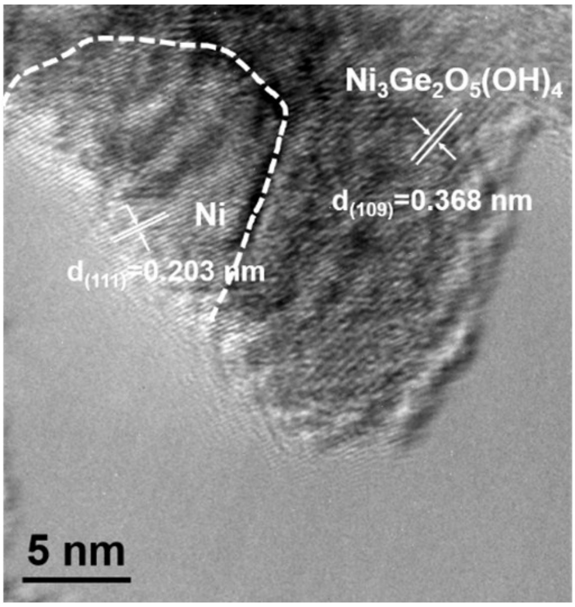

Fig. S4. HR-TEM lattice image of $Ni_3Ge_2O_5(OH)_4$ after annealing treatment for 1 h at 673 K under flowing N_2.

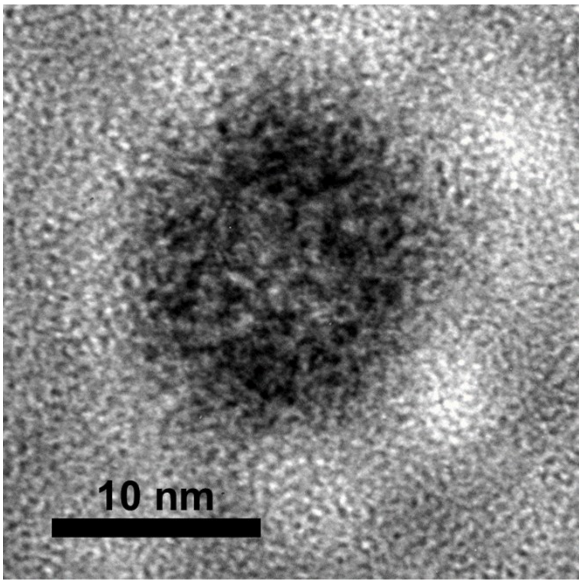

Fig. S5. HR-TEM image of Ni nanoparticles. Ni nanoparticles were prepared by direct reduction of $Ni(NO_3)_2$ by $NaBH_4$ solution at 273 K.

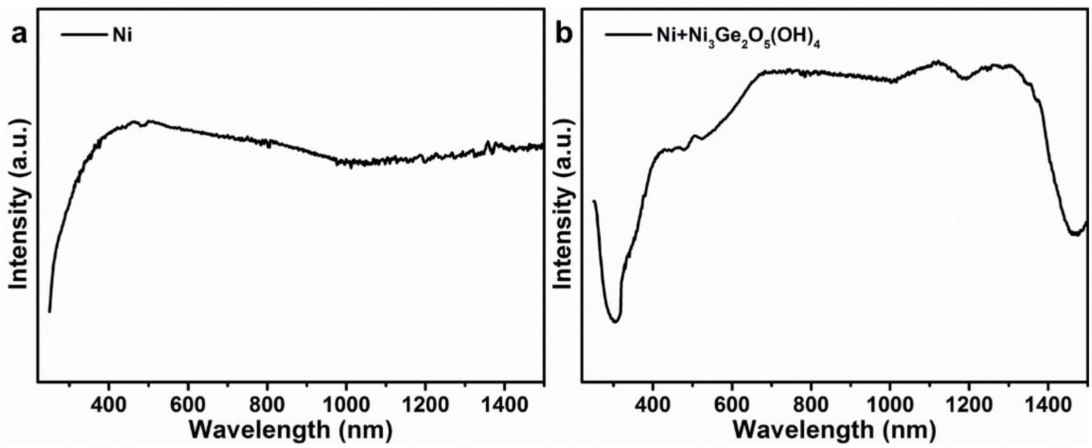

Fig. S6. (a) UV-vis adsorption spectra for Ni nanoparticles and (b) $Ni+Ni_3Ge_2O_5(OH)_4$. Ni nanoparticles were prepared by direct reduction of $Ni(NO_3)_2$ by $NaBH_4$ at 273K. $Ni+Ni_3Ge_2O_5(OH)_4$ was prepared by mechanical grinding of Ni nanoparticles and $Ni_3Ge_2O_5(OH)_4$ according to the mole ratio of Ni^{2+} to Ni^0 in $Ni/Ni_3Ge_2O_5(OH)_4$.

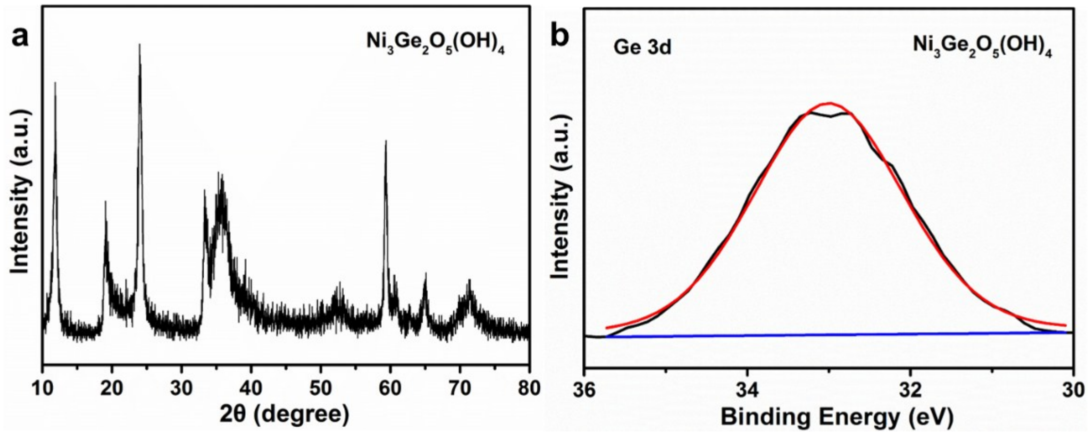

Fig. S7. (a) XRD pattern and (b) Ge 3d XPS spectrum of $Ni_3Ge_2O_5(OH)_4$ with high crystalline. $Ni_3Ge_2O_5(OH)_4$ with high crystalline was prepared by hydrothermal method (453 K for 12h).

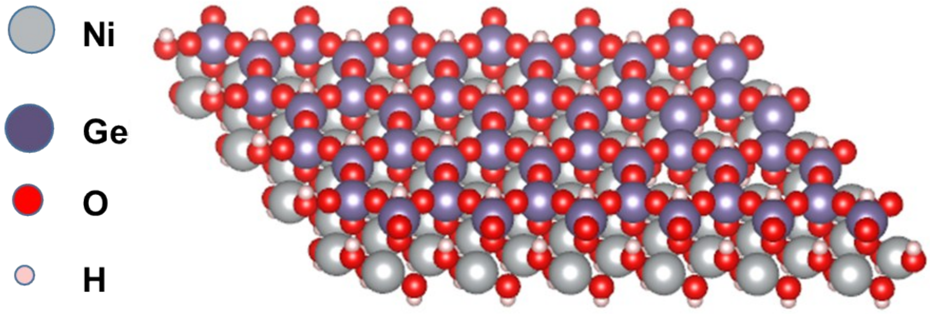

Fig. S8. Crystal structure of $Ni_3Ge_2O_5(OH)_4$.

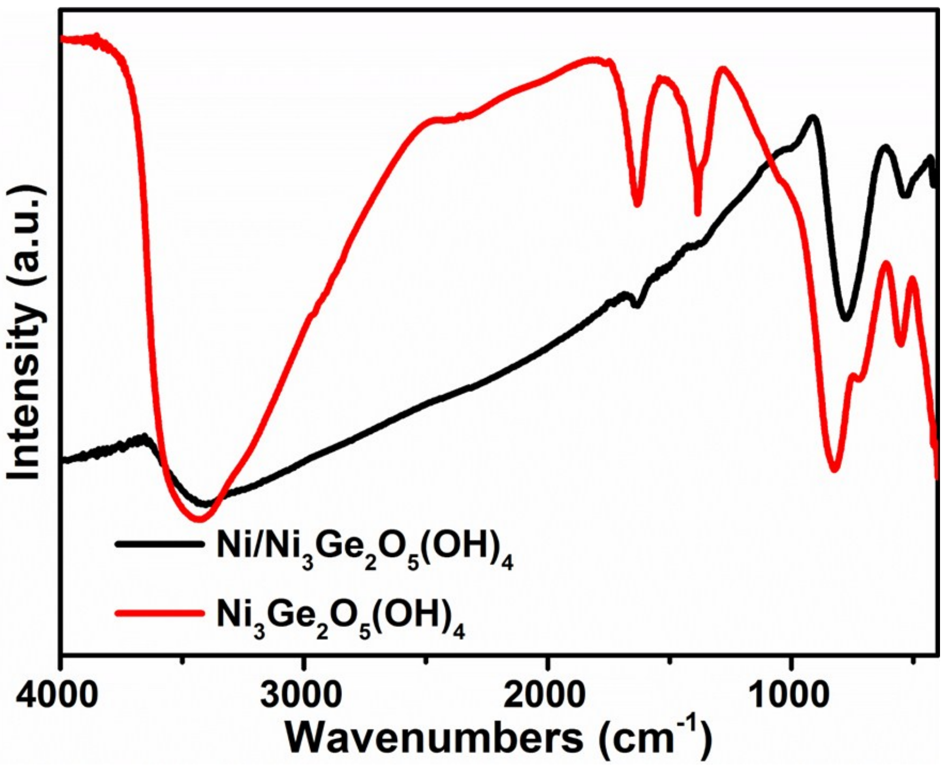

Fig. S9. Quantitative FT-IR spectrum of $Ni/Ni_3Ge_2O_5(OH)_4$ and $Ni_3Ge_2O_5(OH)_4$.

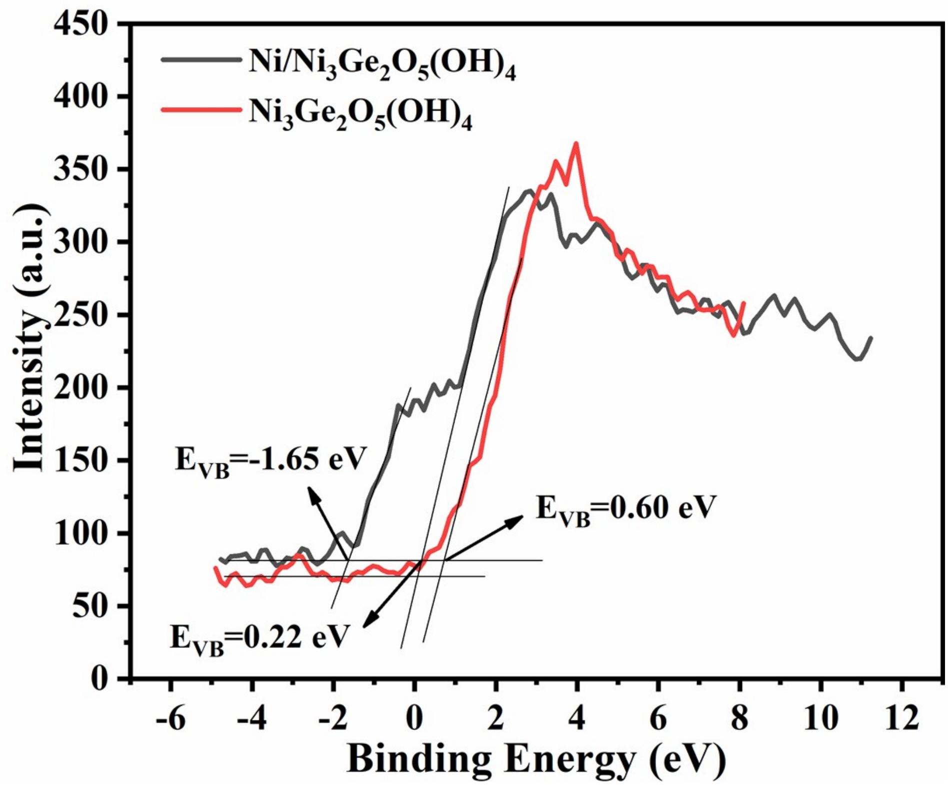

Fig. S10. Valence-band XPS spectra of $Ni/Ni_3Ge_2O_5(OH)_4$ and $Ni_3Ge_2O_5(OH)_4$.

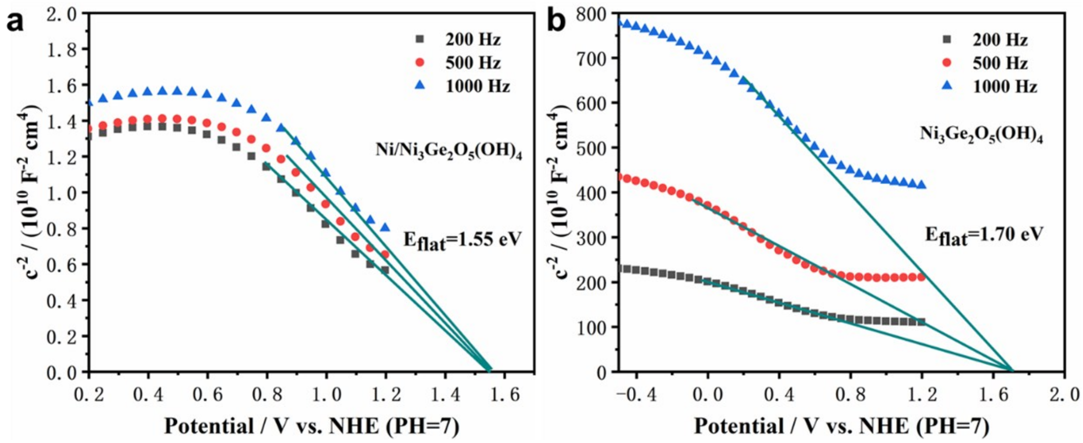

Fig. S11. Mott-Schottky plots for (a) $Ni/Ni_3Ge_2O_5(OH)_4$ and (b) $Ni_3Ge_2O_5(OH)_4$ in 0.5 M Na_2SO_4 aqueous solution with frequencies of 200 Hz, 500 Hz and 1000 Hz.

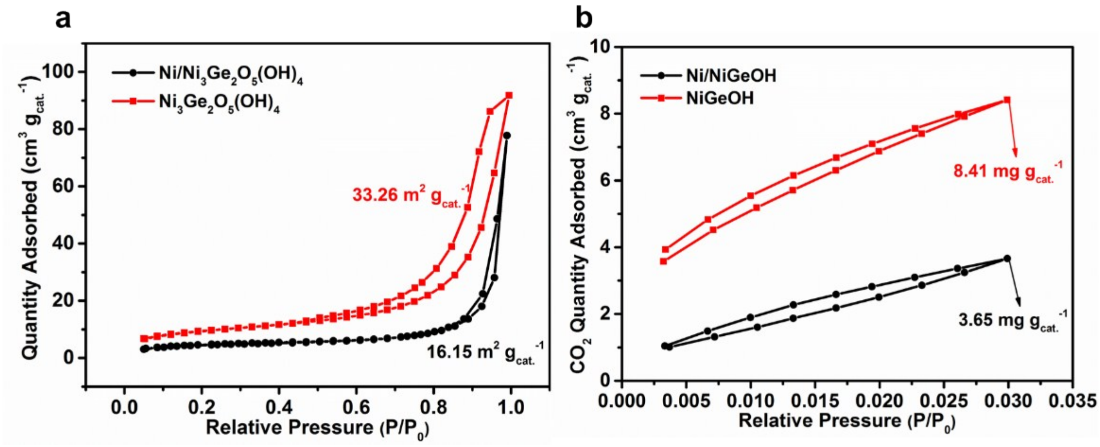

Fig. S12. (a) Specific surface area (b) and CO_2 adsorption quantity for the $Ni/Ni_3Ge_2O_5(OH)_4$ and $Ni_3Ge_2O_5(OH)_4$, respectively.

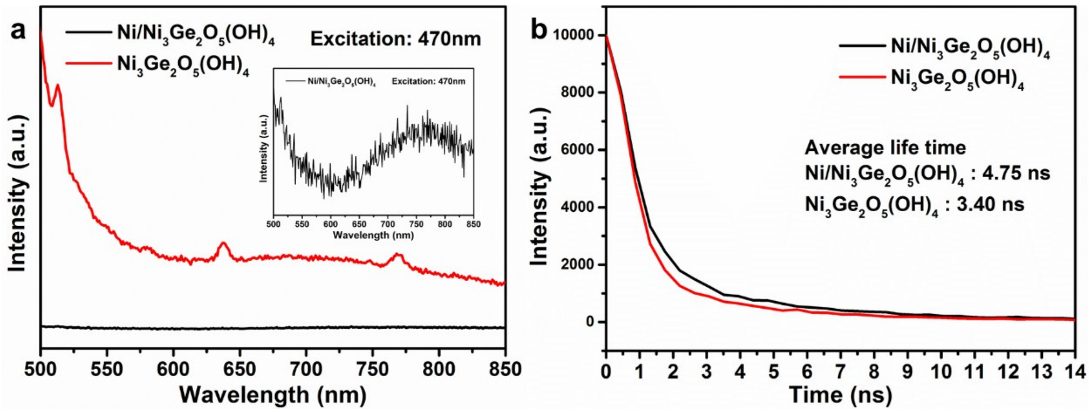

Fig. S13. (a) Steady-state photoluminescence spectra of $Ni/Ni_3Ge_2O_5(OH)_4$ and $Ni_3Ge_2O_5(OH)_4$ under the excitation of 470 nm. (b) PL decay traces of $Ni/Ni_3Ge_2O_5(OH)_4$ and $Ni_3Ge_2O_5(OH)_4$ and their corresponding fluorescence lifetimes under the excitation of 470 nm. The inset in Figure S11a showed the enlarged PL spectrum for $Ni/Ni_3Ge_2O_5(OH)_4$.

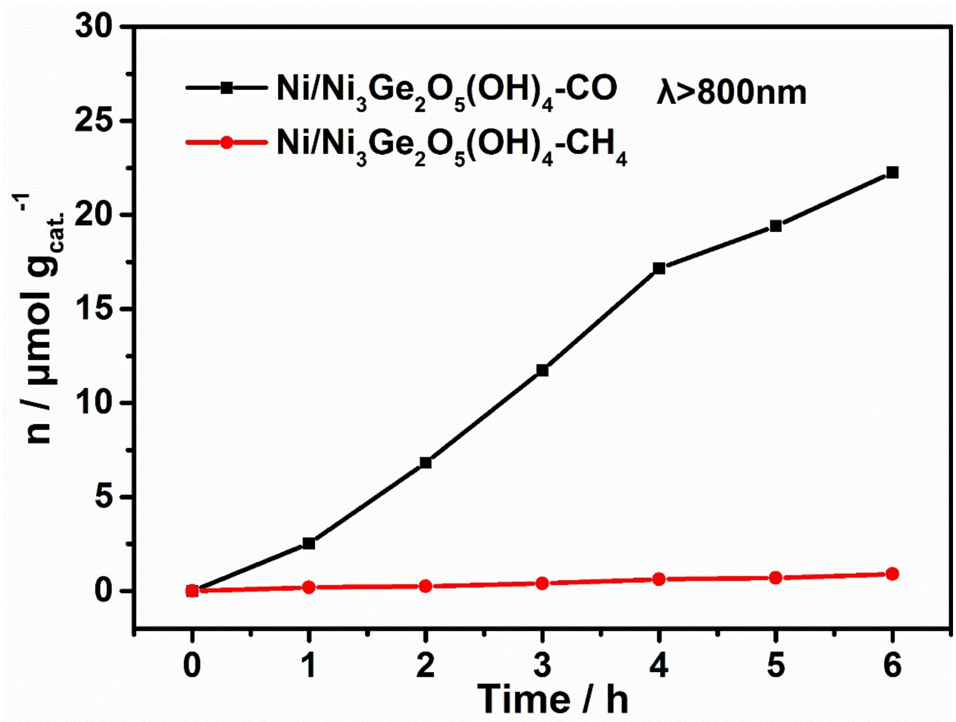

Fig. S14. CO and CH_4 yields for $Ni/Ni_3Ge_2O_5(OH)_4$ under infrared light irradiation for 6 h.

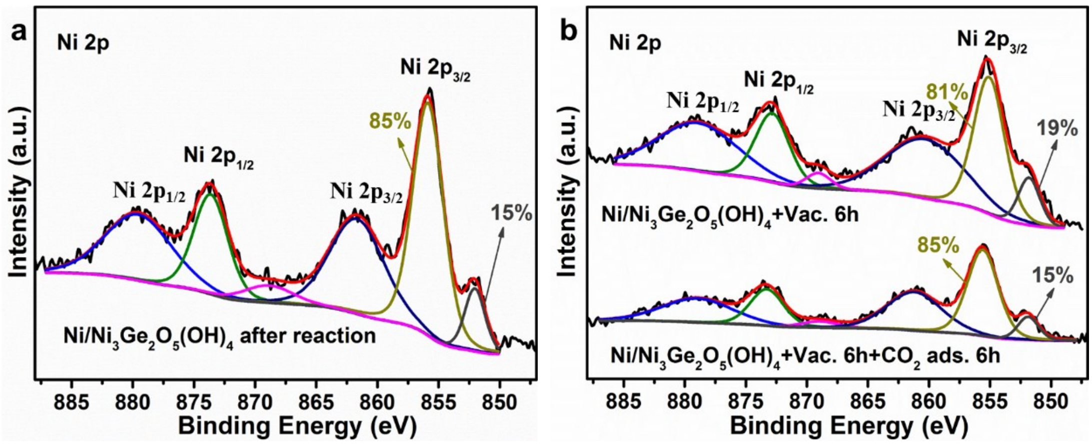

Fig. S15. (a) Ni 2p XPS spectra for Ni/$Ni_3Ge_2O_5(OH)_4$ after reaction. (b) Ni 2p XPS spectra for Ni/$Ni_3Ge_2O_5(OH)_4$+Vac.6h and Ni/$Ni_3Ge_2O_5(OH)_4$+Vac.6h+CO_2 ads.6h.

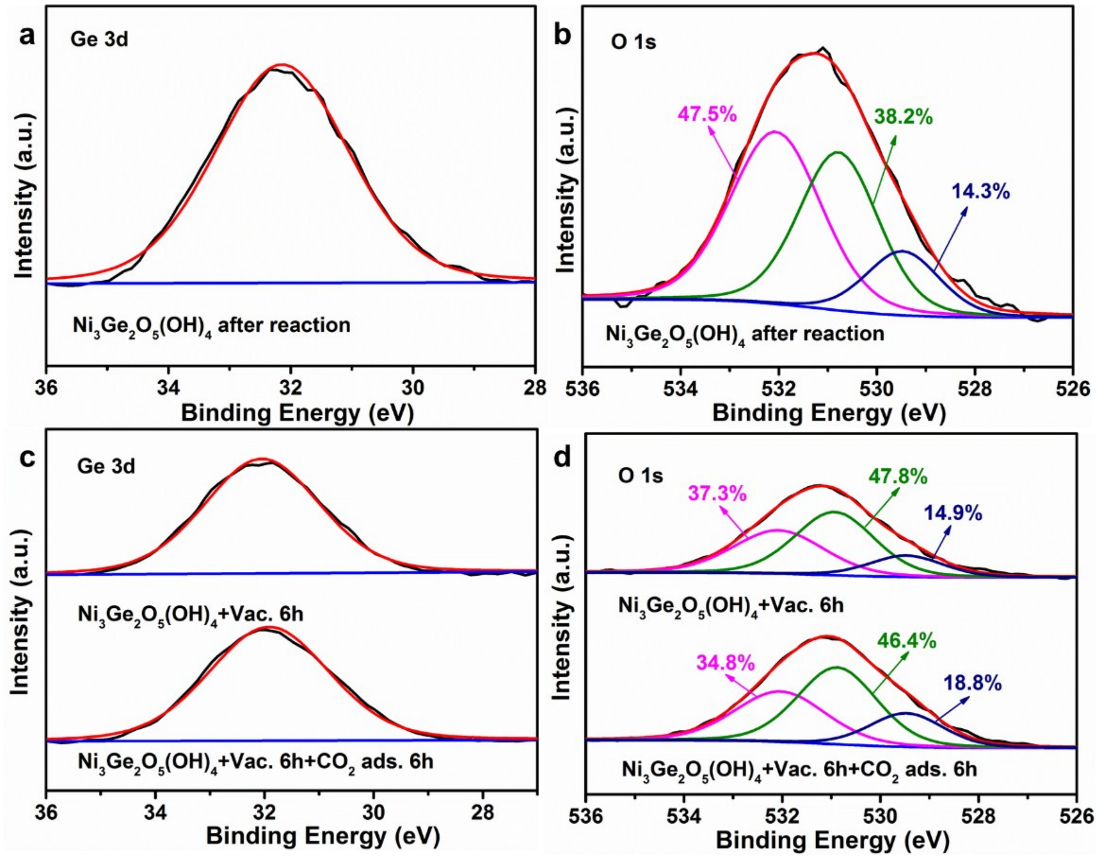

Fig. S16. (a) Ge 3d and (b) O 1s XPS spectra for $Ni_3Ge_2O_5(OH)_4$ after reaction. (c) Ge 3d and (d) O 1s XPS spectra for $Ni_3Ge_2O_5(OH)_4$ after vacuum irradiation for 6 h (denoted as $Ni_3Ge_2O_5(OH)_4$+Vac.6h) and for $Ni_3Ge_2O_5(OH)_4$+Vac.6h after CO_2 adsorption for 6 h (denoted as $Ni_3Ge_2O_5(OH)_4$+Vac.6h+CO_2 ads.6h).

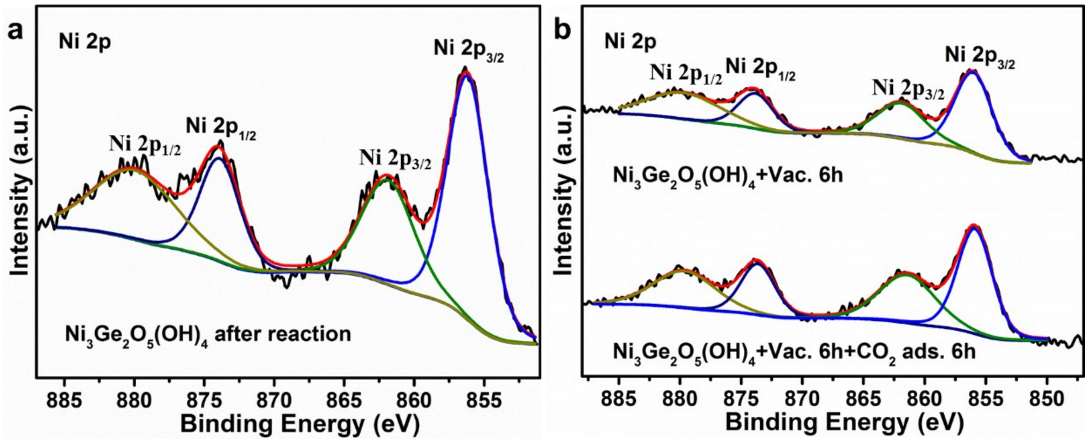

Fig. S17. (a) Ni 2p XPS spectra for $Ni_3Ge_2O_5(OH)_4$ after reaction. (b) Ni 2p XPS spectra for $Ni_3Ge_2O_5(OH)_4$+Vac.6h and $Ni_3Ge_2O_5(OH)_4$+Vac.6h+CO_2 ads.6h.

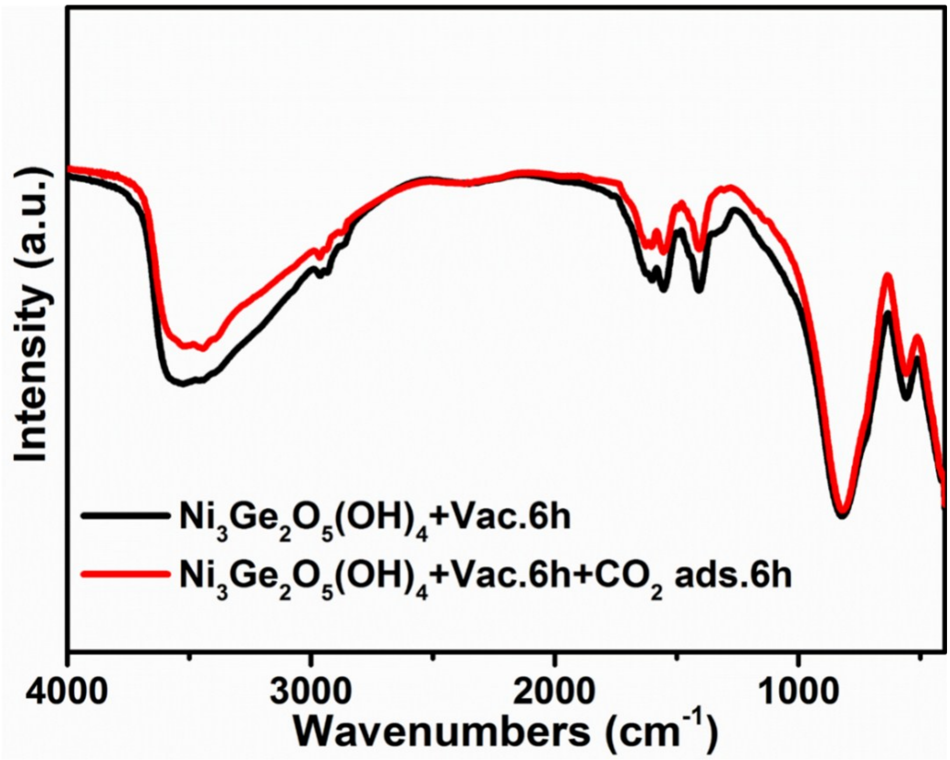

Fig. S18. FT-IR pattern for $Ni_3Ge_2O_5(OH)_4$+Vac.6h and $Ni_3Ge_2O_5(OH)_4$+Vac.6h+CO_2 ads.6h.

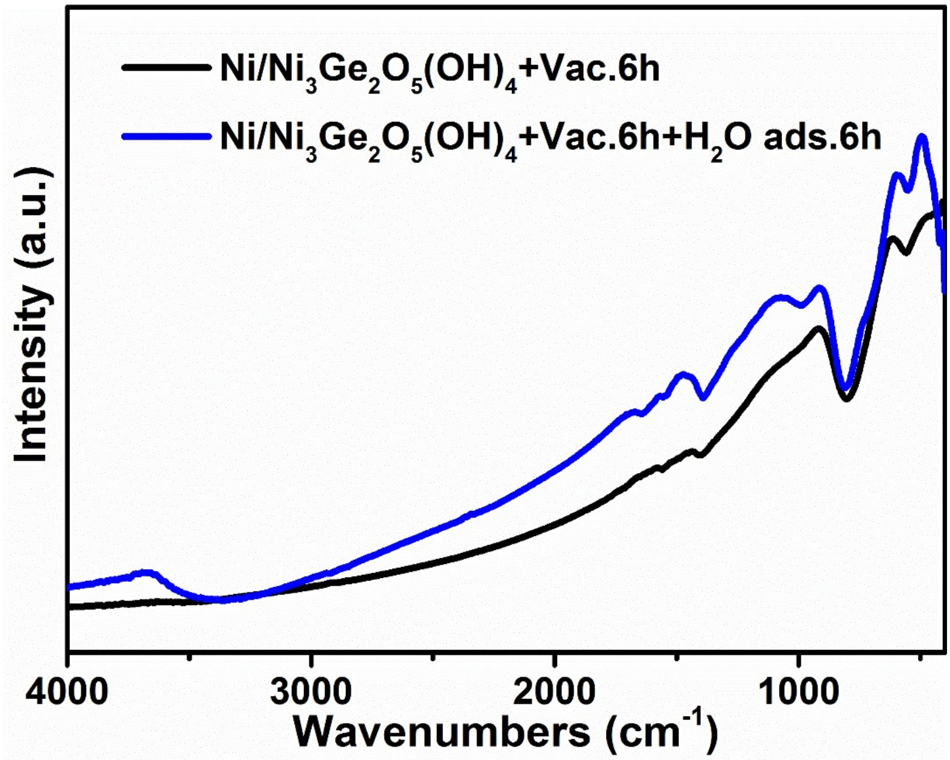

Fig. S19. FT-IR spectra of $Ni/Ni_3Ge_2O_5(OH)_4$+Vac.6h and $Ni/Ni_3Ge_2O_5(OH)_4$+Vac.6h after H_2O adsorption for 6h (denoted as $Ni/Ni_3Ge_2O_5(OH)_4$+Vac.6h+H_2O ads.6h).

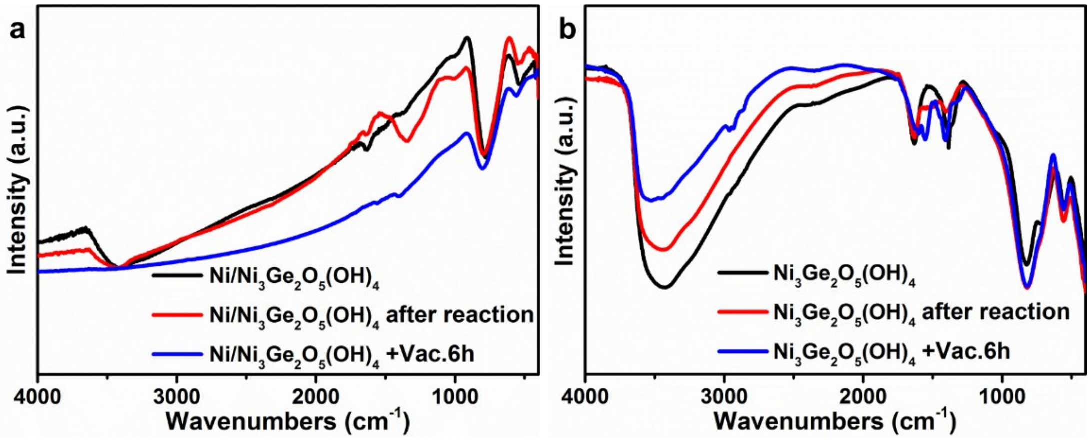

Fig. S20. (a) FT-IR pattern of $Ni/Ni_3Ge_2O_5(OH)_4$, $Ni/Ni_3Ge_2O_5(OH)_4$ after reaction, $Ni/Ni_3Ge_2O_5(OH)_4$+Vac.6h. (b) FT-IR pattern of $Ni_3Ge_2O_5(OH)_4$, $Ni_3Ge_2O_5(OH)_4$ after reaction, $Ni_3Ge_2O_5(OH)_4$+Vac.6h.

Table S1. The gas yield of O_2 of $Ni/Ni_3Ge_2O_5(OH)_4$ and $Ni_3Ge_2O_5(OH)_4$

Photocatalysts	**Condition**	**O_2 yield (μmol $g_{cat.}^{-1}$)**
$Ni/Ni_3Ge_2O_5(OH)_4$	Visible-light irradiation for 1h	1472
$Ni_3Ge_2O_5(OH)_4$	under vacuum	37
$Ni/Ni_3Ge_2O_5(OH)_4$	Visible-light irradiation for 6h	1692
$Ni_3Ge_2O_5(OH)_4$	under vacuum	82
$Ni/Ni_3Ge_2O_5(OH)_4$	Visible-light CO_2 reduction	897
$Ni_3Ge_2O_5(OH)_4$	for 1h	14